RSC Advances

RSC Publishing

PAPER

Water-triggered shape memory of multiblock thermoplastic polyurethanes (TPUs)†

Cite this: *RSC Advances*, 2013, **3**, 15783

Xinzhu Gu and Patrick T. Mather*

In this article we describe the preparation and characterization of a water-triggered shape memory polymer (SMP) family, PCL–PEG based thermoplastic polyurethanes (TPUs). Upon immersion in water, water molecules selectively swelled the hydrophilic PEG domains, resulting in durable hydrogels with strain-to-failure values greater than 700%. Dry samples fixed in a temporary shape underwent water-triggered shape recovery wherein only the oriented PEG domains recovered, causing incomplete shape recovery toward the equilibrium shape upon contact with liquid water. Addressing the limited recovery observed for dry-fixing samples that led to some PCL domain deformation, we developed a novel, ''wet-fixing'' SM cycle, where the temporary shape is achieved by deforming the material in the hydrogel state (wet drawing) and is later fixed *via* PEG recrystallization upon drying. The fixing and recovery ratios were substantially improved using this new shape memory programming method, the mechanism of which was proven by X-ray diffraction analysis. The recovery speed of this material system was studied by varying the thickness of bulk films and demonstrated that water-recovery is diffusion-limited. By processing the TPUs as a web of microfibers, rapid shape recovery was achieved in water at room temperature within 1.3 s. The controllable actuation speed, the high recoverable strain, and the simple fixing and recovery process make these materials potential candidates for applications as water responsive sensors, actuators, and medical devices.

Received 19th March 2013,
Accepted 25th June 2013

DOI: 10.1039/c3ra41337c

www.rsc.org/advances

Introduction

Shape memory polymers (SMPs) are a class of stimuli-responsive materials that can be elastically deformed and subsequently fixed into a temporary shape by network chain immobilization, and later recover to their original (permanent) shape when exposed to external stimuli that re-mobilize the network chains. Direct heating is the most widely studied external stimulus to induce shape recovery in the past years.[1] Other stimuli such as light,[2] electricity,[3] magnetic field,[4] and moisture[5] have also been utilized as the recovery triggers.

Compared with heat-triggered SMPs, water responsive SMPs are capable of regaining their original shapes simply by immersing the samples in water. Here undesirable effects resulting from external heating, such as damage of surrounding tissue and cells when activating a smart implant, can be avoided. In 2003, Yang and co-workers[6] accidentally found that a pre-deformed and fixed film made of a commercially available polyurethane (T_g = 35 °C) became rubber-like after one month of exposure in air at room temperature and recovered its original shape, with the T_g decreasing to about 22 °C. Later, moisture was identified as the stimulus causing the polymer to become rubber-like and thus triggering the shape recovery. This research group also unveiled the recovery mechanism: water molecules, which diffuse into the polymer sample, disrupt the intramolecular hydrogen bonding and mobilize the previously vitrified network chains, thereby shift SMP transformation temperature (here, T_g) to lower temperatures and allow for room temperature actuation.[5,7] The shape-memory effect associated with the lowering of transition temperatures has also been shown for polyurethanes composites with carbon nanotubes.[8] In all cases, the shape memory effect was slow, with recovery taking at least 140 min.

A different strategy for water-induced shape-memory polymers has been realized by incorporating a hydrophilic or water swellable component into the structure. In this way, the shape recovery can be greatly accelerated. Jung and co-workers[9] demonstrated the water-activated SM effect in poly(ethylene oxide) (PEO)-based polyurethanes with the hydrophobic polyhedral oligosilsesquioxane (POSS) moiety as the hard-

Syracuse Biomaterials Institute and Department of Biomedical and Chemical Engineering, Syracuse University, Syracuse, USA. E-mail: ptmather@syr.edu; Fax: (315) 443-9175; Tel: (315) 443-8760

† Electronic supplementary information (ESI) available: The swelling and deswelling kinetics at room temperature for one representative composition, $[PCL]_{50}$–$[PEG]_{50}$; Asymptotic dependence of strain recovery on PEG wt%; WAXS analysis of hydrated samples revealing only PCL crystal reflections; SEM analysis of fibrous web; Effect of fixing time on wet-fixing quality; 2D WAXS patterns for deformed and fixed samples; Azimuthal profiles of WAXS data for deformed and fixed samples; Orientation degree measurements for PCL and PEG reflections; Movies revealing water-triggered recovery; Table with comparison of mechanical properties of synthetic and natural hydrogels reported in the literature. See DOI: 10.1039/c3ra41337c

segment. Exposure to water resulted in the water-swelling of the PEG segment and recovery of the permanent shape. The polymer films, obtained by solution casting, showed incomplete recovery (65–85%) after 300 s at 35 °C water. By modifying chitosan with PEG and epoxide crosslinking, Chen and co-workers[10] prepared a water-activated biodegradable stent. The equilibrium shape was chemically fixed by crosslinking. The raw materials (chitosan and polyethylene glycol) used were relatively hydrophilic, and a subsequent immersion in water led to rapid hydration and recovery in a short period of 150 s. Shape memory polymers sensitive to organic solvents can also be obtained which is similar to the hydrophilic SMPs that are sensitive to water. Lv *et al.*[11] and Lu *et al.*[12] observed that dimethyl formamide (DMF) was capable of activating the shape memory response of a styrene-based SMP. Again, this effect was slow, with recovery taking at least 180 min.

The slow response of existing water-triggering shape memory systems has indicated the need for new material design strategies that could tailor the recovery speed and recovery ratios for more controlled actuation. Recently, we prepared a series of high molecular weight, water sensitive multiblock polyurethanes consisting of PCL and PEG. In this system, instead of conventional ''hard'' blocks, entanglements serve as the physical crosslink in this system, which gives excellent elasticity above the melting transition. As such, the materials demonstrated excellent heat-triggered shape memory upon heating.[13] In the present study, water-triggered shape memory was investigated for this family of PCL–PEG TPUs. A new, ''wet-fixing'' shape memory cycle was developed to improve shape memory performance (*i.e.* fixing and recovery abilities), and the mechanism was understood by X-ray analysis. Furthermore, the rate of water triggering was manipulated through variation of the diffusion distance in the form of bulk film thickness. Finally, we demonstrate that the rate of water triggering can be greatly accelerated through a significant decrease in the diffusion distance, which was realized through the processing of selected SMPs in the form of nano- or micro- fibrous webs instead of bulk films.

Experimental section

Synthesis and molding

The synthesis and characterization of high molecular weight PCL–PEG multiblock hybrid thermoplastic polyurethanes were described in our previous report.[13] The molecular weight of both PEG and PCL blocks is kept at 10 kg mol^{-1} for all the polymers, and this characteristic is not designated in the sample nomenclature for simplicity. The feed molar ratios of PCL/PEG blocks are indicated as subscripts in the naming system. As an example, $[PCL]_{50}$–$[PEG]_{50}$ designates a multiblock copolymer consisting of PCL (10 kg mol^{-1}) and PEG (10 kg mol^{-1}) blocks with a feed weight percent ratio of 50 : 50. Films were made from as-synthesized polymers using a Carver 3851-0 hydraulic press with custom, temperature-controlled heating platens. In particular, polymer powder was sandwiched between two Teflon sheets with a Teflon spacer placed in between the sheets. A compressive stress of 0.4 MPa was applied at 90 °C and held for 30 s. Then, the platens were cooled to room temperature (RT), assisted by cooling water, following which the compressive stress was released. Teflon spacers with different thicknesses were used to control the thickness of the films, which were later determined using a digital caliper.

Electrospinning

Electrospinning solutions were prepared by dissolving PCL–PEG TPUs (0.8 g) in a mixed THF/DMF solvent (V_{THF} : V_{DMF} = 1 : 1, V_{total} = 8 mL). The electrospinning setup consisted of a syringe pump (KDS100, KD Scientific), a high voltage power supply unit (modulated by a low voltage, Agilent E3630A DC power supply), and a custom-made rotating drum collector. A voltage of 13 kV, a flow rate of 0.3 mL h^{-1} and a needle-to-collector distance of 10 cm were used. Aluminum foil was placed on the drum for fiber collection. The drum, with diameter of 5 cm, was rotated at 400 rpm with a slow lateral translation over a distance of 5 cm, yielding mats with relatively uniform thickness. Samples for microscopy were coated with gold using a Denton Vacuum-Desk II gold sputter coater and the surface morphology was investigated using a JEOL JSM5600 scanning electron microscope (SEM) instrument.

Swelling measurements

To characterize the swelling behavior of the hot-press films and e-spun webs in water, samples were cut into square pieces with typical dimensions of 10 mm × 10 mm, and were then immersed in water at room temperature for 1 h. Then, the samples were taken out and patted dry. Water uptake and volume expansion were quantified using eqn (1) and eqn (2):

$$\text{Water uptake (\%)} = \left(\frac{m_w - m_d}{m_d}\right) \times 100 \quad (1)$$

$$\text{Volume expansion (\%)} = \left(\frac{V_w - V_d}{V_d}\right) \times 100 \quad (2)$$

where m_d and V_d are the mass and volume of the original dry films, and m_w and V_m are the mass and volume of the wet samples, respectively. Average values for three samples (n = 3) are reported herein, with the error bars indicating one standard deviation.

Mechanical properties

The ultimate tensile properties of films and e-spun webs, in both dry state and hydrogel (wet) state, were studied using a Linkam TST-350 tensile testing system with a 20 N (0.01 N resolution) load cell at room temperature. Each sample was punched into a dogbone geometry using an ASTM Standard D638-03 Type IV (scaled down by a factor of 4). This dogbone geometry was employed for all the following mechanical testing and shape memory characterization unless otherwise mentioned. For hydrogel testing, samples were immersed in water until they reached equilibrium prior to cutting with the dogbone die. Sand paper was used to increase the friction between the hydrogels and the clamps so that no slipping

occurred during the measurements. Samples were extensionally deformed with a crosshead speed of 200 μm s^{-1} (192% min^{-1}) at room temperature until fracture occurred. Young's modulus was calculated by finding the initial slope of the stress *versus* strain curve ($0 < \varepsilon < 10\%$) using linear regression. The ultimate stress was reported as the highest stress in the stress-strain curve, and the strain-at-break was recorded as the strain at the point where the force became zero. The experiment was repeated three times for each material, with typical results presented graphically and average values reported.

Microstructural characterization

The microstructure of the samples in the deformed and recovered states were studied using wide angle X-ray scattering (WAXS) with a Rigaku S-MAX3000 (Woodlands, TX). A MicroMax-002+ High-Intensity Microfocus Sealed Tube X-ray Generator was used to produce a beam of collimated Cu-Kα X-ray radiation with a wavelength of 1.5405 Å. An accelerating voltage of 45 kV and a current of 0.88 mA were applied. The scattered X-ray patterns were collected using a FujiFilm FLA7000 reader. The distance between sample and image plate was fixed at 120 mm for WAXS collection and exposure times of 30 min were utilized. Samples were exposed under vacuum to eliminate air exposures.

Water-triggered shape memory characterization

Samples for water-triggered shape memory testing were deformed using Linkam tensile tester. Specimens were stretched at room temperature to a strain of ε_m at a rate of 192% min^{-1}. The strain was then decreased at 192%/min until the force reached zero, after which a large percentage of plastic strain remained (ε_u). Shape recovery was then induced by immersing the deformed samples in water at RT for 10 min to a recovered strain, ε_r, which was calculated using $\varepsilon_r = (L_r - L_0)/L_0 \times 100$, where L_r is the gauge length of the recovered sample, and L_0 is the gauge length of the original sample (6.25 mm here). The fixing (R_f) and recovery (R_r) ratios were calculated using eqn (3) and eqn (4). The experiment was conducted three times per material.

$$R_f = \left(\frac{\varepsilon_u}{\varepsilon_m}\right)\cdot 100 \quad (3)$$

$$R_r = \left(\frac{\varepsilon_u - \varepsilon_r}{\varepsilon_u}\right)\cdot 100 \quad (4)$$

To characterize the recovery kinetics, pre-stretched samples were placed into RT water with a light screw (3 g) hung on one end of the samples to keep the samples straight during recovery. A high speed camera (Fastcam-512PCI, Photron) with a sampling rate of 60 or 250 frames per second was used to image samples during recovery. Recovery ratios (R_r) were calculated by eqn (4), where L_r of selected frame was measured using ImageJ software (1.44 p).

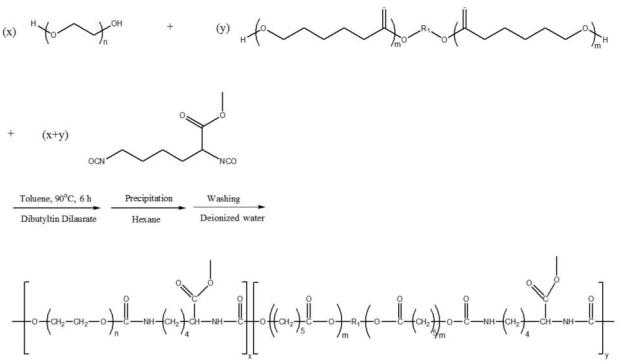

Scheme 1 Preparation of PCL–PEG multi-block TPUs by reacting the PEG diol and PCL diol with a lysine-derived diisocyanate.

Results and discussion

The synthesis of high molecular weight PCL–PEG multiblock hybrid thermoplastic polyurethanes is shown schematically in Scheme 1. The urethane linkages were formed through the addition reaction between isocyanate groups of the lysine methyl-ester diisocyanate (LDI) and the hydroxyl groups of either poly(ethylene glycol) (PEG) or poly(ε-caprolactone) (PCL) diol. Seven PCL–PEG TPUs of varying compositions were synthesized. The feed ratios of PCL/PEG were varied to control the hydrophilic–hydrophobic balance. The basic material properties for these polyurethanes were reported in our previous study.[13] Crystalline phases of both blocks coexisted in the multi-block TPUs, indicating micro-phase separation driven by thermodynamic incompatibility between hydrophilic PEG blocks and hydrophobic PCL blocks and dramatic contrast in hydrophilicity between the two blocks.

The study of the water-triggered shape memory behavior of PCL–PEG TPUs involves their contact with water. As such, their water-swelling behaviors are of primary importance. Here, water was expected to selectively permeate into the hydrophilic PEG blocks, resulting in weight gain of the bulk materials. The hydrophobic PCL-rich domains and the entanglements serving as physical crosslinks prevented the material from dissolution, limiting swelling. For the two homopolymers, $[PCL]_{100}$ exhibited almost no water uptake, while $[PEG]_{100}$ dissolved in water upon immersion. In contrast, the copolymers swelled in water, evidenced by mass gain and volumetric expansion. It was found that the weight gain of the five copolymers increased from 26% ($[PCL]_{70}$–$[PEG]_{30}$) up to 311% ($[PCL]_{30}$–$[PEG]_{70}$) with increasing PEG content, as shown in Fig. 1. The weight gain was quite close to volume expansion, as expected due to the density of our TPUs being similar to water. All of the hydrogels were translucent in appearance, a finding we attribute to the microphase-separated structure and high crystallinity of the water-impervious PCL blocks. The swelling and deswelling kinetics at room temperature for one representative composition, $[PCL]_{50}$–$[PEG]_{50}$, are provided in Fig. S1, ESI†. After 2 min in water, more than 60% water had permeated into the sample. Equilibration was reached within

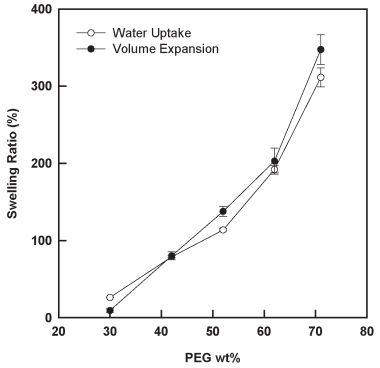

Fig. 1 Water uptake and volume expansion of PCL–PEG TPUs hot-press films. Films were immersed in water at room temperature for 1 h.

8 min and settled at a value of 120%. Upon drying in open atmosphere, the absorbed water gradually evaporated and the sample was completely dried within 2 h.

The fixed strains of stretched films were expected to partially recover upon immersion in water, considering water only dissolves the hydrophilic PEG domains. Thus, copolymers films were stretched to 1240% at RT using the Linkam tensile tester and the strains were then released until the stresses dropped to 0 MPa, to observe the initial elastic shape recovery. This yielded fixed deformations between permanent and temporary shape to be ~800%. Upon tensile deformation, the constituent chains and domains of both PCL and PEG phases became highly oriented. All compositions completed their water-triggered recovery within 10 min, with the extent of recovery increasing from 8% to 47% as the PEG content increased from 30 to 70 wt% (Fig. 2, Table 1). The asymptotic dependence of recovery on PEG wt% (Fig. S2, ESI†) is explained by the higher swelling ratios at higher PEG content. The swelling trend was clearly reflected by tab parts of the dogbone samples after water recovery (Fig. 2). Only PCL crystal reflections existed in the wet state and they remained oriented after water-triggered recovery based on the WAXS results (Fig. S3, ESI†). This indicates, interestingly, that the deformed PCL phase is the root cause of incomplete recovery of copolymers in water, and suggests the solution introduced later in this manuscript: wet drawing. In addition, the PCL peaks became broader in the wet state, implying the decrease of crystallite

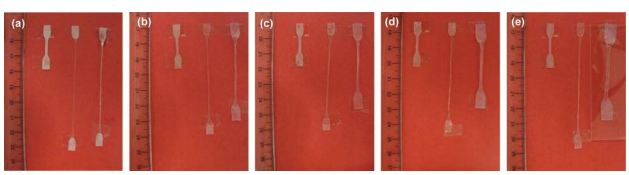

Fig. 2 Water-triggered shape memory tests of PCL–PEG TPUs hot-pressed film: (a) $[PCL]_{70}$–$[PEG]_{30}$, (b) $[PCL]_{60}$–$[PEG]_{40}$, (c) $[PCL]_{50}$–$[PEG]_{50}$, (d) $[PCL]_{40}$–$[PEG]_{60}$, and (e) $[PCL]_{30}$–$[PEG]_{70}$. Samples on the left of each pictures: original dogbone films; samples shown in the middle: deformed films by Linkam; samples on the right: films after deformation by Linkam and then water recovery at room temperature for 10 min.

Table 1 Summary of fixing ratios (R_f %) films after deformation and water recovery at room temperature and recovery ratios (R_r %) of PCL–PEG TPUs, which were deformed by Linkam and recovered in water at RT for 10 min

Material	R_f (%)	R_r (%)
$[PCL]_{70}$–$[PEG]_{30}$	72 ± 3	8 ± 2
$[PCL]_{60}$–$[PEG]_{40}$	58 ± 3	29 ± 2
$[PCL]_{50}$–$[PEG]_{50}$	59 ± 3	39 ± 2
$[PCL]_{40}$–$[PEG]_{60}$	60 ± 6	46 ± 2
$[PCL]_{30}$–$[PEG]_{70}$	71 ± 4	47 ± 3

size after immersing in water. It is noted that the strains used in our shape memory characterizations are from crosshead displacement. As such, the reported strains are likely larger than actual strains within the Type IV dogbone gauge length.

Some of the key limitations of the current PCL–PEG TPUs system include: (1) low recovery ratio (<50%), primarily due to unrecovered PCL phase in water; (2) Low recovery speed. Although the recovery speed is already quite high among the current water-triggered SMPs in literature, it's still not comparable to that of heat-induced SMPs[14] or electrically-triggered SMPs[3], the recovery of which completes in a couple of seconds. The limitations of current PCL–PEG TPUs indicated the need for new material and process design strategies that could improve the recovery ratios and enhance the recovery speed. $[PCL]_{40}$–$[PEG]_{60}$ was picked as the material for all the following study given its relatively good water recovery property.

Given the time scale for mass diffusion follows $\tau \approx d^2/D$, where d is the diffusional distance and D is the mass diffusivity, one hypothesis we have is that the rate of water triggering can be sped up through a significant decrease in the diffusion distance. We reasoned that this could be accomplished through the processing of $[PCL]_{40}$–$[PEG]_{60}$ in the form of nano- or micro- fibers. The fibrous mats were achieved by electrospinning with an average thickness of 0.38 mm, which is comparable to the thickness of the bulk films (0.35 mm), but with much smaller internal structure of the constituent fibers. Electrospinning has been widely studied for producing polymeric micro- and nano-fibers.[15,16] Electrostatic forces are utilized to uniaxially stretch a viscoelastic jet derived from a polymer solution or melt into fibers with small diameters. The resulting electrospun fibrous mats made from the PCL–PEG TPUs had the appearance of a white, nonwoven fabric. The fiber morphology was further characterized by SEM, and a representative micrograph is shown in Fig. S4, ESI†. Using ImageJ software, an average fiber diameter of 810 ± 28 nm was obtained from 90 measurements.

Fig. 3a shows the volume expansion of a hot-press film after reaching the equilibrium state. In contrast, the electrospun fibrous mats did not expand upon exposure to water, as shown in Fig. 3b. We suggest that the relaxation of molecular orientation upon hydration suppressed swelling characteristics in the radial direction. Owing to the internal void space in the porous structure, the water uptake of the webs (840%) was much higher than that of the films (192%) (Table 2). Similar

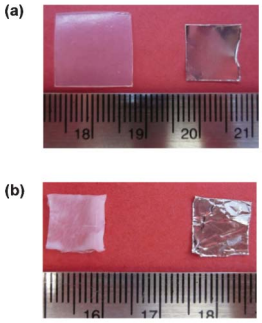

Fig. 3 Digital images of (a) hot-pressed films (hpf) and (b) electrospun webs in the water swollen state. The aluminum foils shown on the right of each image represent the dimensions of samples in the dry state. Samples were immersed in water at room temperature for 10 min.

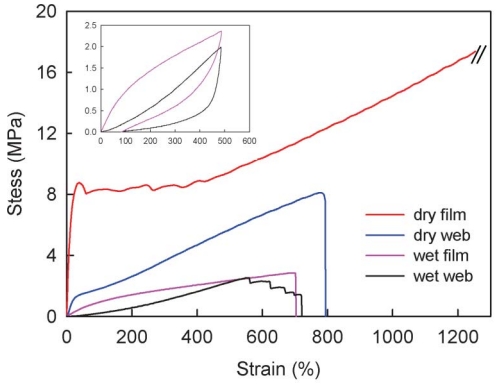

Fig. 4 Stress-strain response of hot-press films and electrospun webs which were stretched in the dry state and wet state, respectively. All samples were deformed at 192% min^{-1} at room temperature. The inset shows hysteresis of two hydrogels (wet film and wet web) upon removal of the load at 192% min^{-1}.

swelling behavior has been reported on the POSS–PEG TPUs system.[17]

Mechanically robust samples were desirable for shape memory applications, so the ultimate tensile properties of films and webs were probed, both in the dry and hydrogel states. For "wet film" and "wet web" specimens, samples were swelled in water to equilibrium first, and then cut into the dogbone geometry. Representative stress-strain curves are provided in Fig. 4, with tensile properties, such as Young's modulus, ultimate tensile stress, and strain-at-break tabulated in Table 3. The stress-strain curve of "dry film" sample is shown as the red curve, with Young's modulus of 56.8 MPa, a yield stress of 9.2 MPa, and a strain-to-failure larger than 1240% (the limit of our apparatus). After immersing the film in water to form a hydrogel (*i.e.* "wet film"), the sample became much softer and gave an elastomeric response with the disappearance of the yield point (pink curve). Its Young's modulus decreased to 1.1 MPa and the strain-to-failure decreased to 735%. When a strain is applied to the dry electrospun mat (blue curve), fibers that happen to be oriented near the strain direction are stretched uniaxially, while most fibers oriented at some angle relative to the stretching direction experience a rotation, resulting in the disappearance of the necking phenomenon, which was previously reported and confirmed here.[18] The orientation of fibers during the initial deformation stage and the lower density of the espun webs lead to the much lower Young's modulus in the electrospun material (the electrospun PU has a density of approximately one-sixth that of the bulk film). The wet e-spun web is the softest among all four samples, with a Young's modulus of 0.2 MPa and an elongation-at-break of 742% (black curve). The failure strain of our hydrogel system is quite high among natural and synthetic hydrogels reported in the literature (Table S1, ESI†).[19–24] The high elongation-at-break would potentially allow large recoverable deformation between the temporary shape and the permanent shape. As shown as an inset in Fig. 4, the two hydrogel samples showed elastomeric behavior, with ~80% strain recovered by releasing the force, though with large hysteresis we attribute to plastic deformation of the hydrophobic PCL phase at room temperature.

Here, we introduce a new, yet simple shape memory cycle that we term "hydrogel shape memory," the idea is shown schematically in Fig. 5 and is explained below. In our PCL–PEG TPUs, both PCL and PEG phases crystallize at room temperature (Fig. 5a). Upon immersion in water, the hydrophilic PEG segments absorb water, and become significantly more compliant than the hydrophobic PCL blocks (Fig. 5b); therefore during wet-drawing, the PEG phase deforms before the PCL phase, the latter undergoes limited or no deformation (Fig. 5c). The temporary, deformed shape is fixed by PEG recrystallization during drying (Fig. 5d). Upon contact with water, the deformed PEG phase recovers, giving rise to near-complete shape recovery (Fig. 5e). In contrast, for a conventional SM cycle, the fixing is accomplished *via* cooling below the transition temperature by vitrification or crystallization after deformation above T_g or T_m. This "hydrogel shape

Table 2 Water uptake, surface expansion and thickness expansion of e-spun webs and hot-press films. Samples were immersed in water at room temperature for 10 min

Samples	Water uptake (%)	Surface expansion (%)	Thickness expansion (%)
Webs	840 ± 8	−2 ± 1	64 ± 13
Films	192 ± 5	146 ± 10	23 ± 2

Table 3 Mechanical properties of e-spun webs and hot-press film in the dry state and in the hydrogel (wet) state

Samples	Young's modulus (MPa)	Ultimate stress (MPa)	Strain at break (%)
Dry films	56.8 ± 2.5	>16	>1240
Dry webs	5.4 ± 1.4	7.0 ± 0.5	820 ± 37
Wet films	1.1 ± 0.2	2.8 ± 0.1	735 ± 39
Wet webs	0.2 ± 0.0	2.4 ± 0.2	742 ± 21

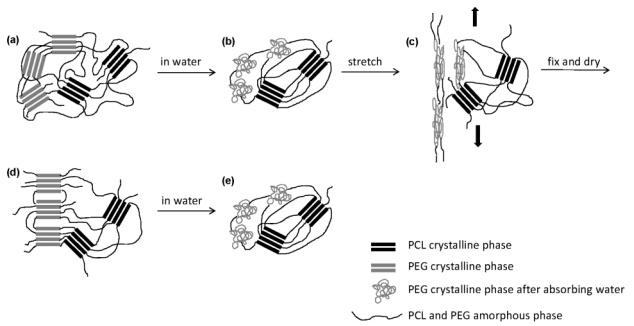

Fig. 5 Schematic illustration of the microstructure change on PCL–PEG TPUs during hydrogel shape memory process.

memory'' hypothesis is proven by comparing the water-triggered recovery behaviors of pre-deformed dry samples and wet samples (hydrogels), as discussed below.

All samples for water-triggered shape memory study were deformed using the Linkam tensile tester at room temperature. The wet film and wet web were stretched to 485% and fixed at this strain by holding for 3 h at room temperature to allow the wet samples to dry and the PEG phase to recrystallize. For comparison, the dry film and dry web were stretched and held at this strain (485%) for 3 h to allow for stress relaxation to occur. The strain was then released until the stress dropped to zero (Fig. 6). Fixing ratios (R_f) for all samples were calculated based on the stress-strain curves and summarized in Table 4. Through fixing *via* PEG recrystallization, both hydrogel samples exhibited higher R_f (89% and 91% for wet film and wet web, respectively) than the dry samples (77% and 70% for dry film and dry web, respectively). The fixing ability of the wet samples was further studied by varying the fixing (drying) time, and it was observed that 1.5 h was long enough to achieve as high R_f as 3 h (Fig. S5, ESI†). These highly deformed samples were then immersed in water at

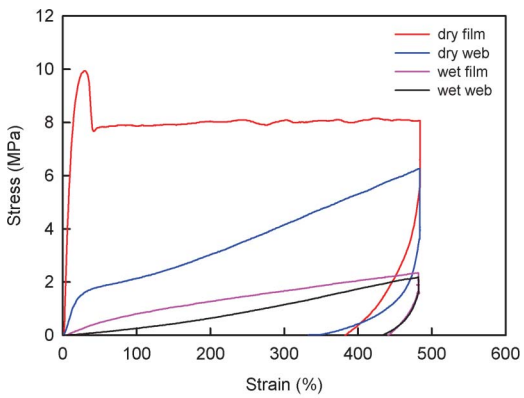

Fig. 6 Stress-strain curves showing the sample programming method for water-triggered shape memory experiments of hot-press film and e-spun webs in dry state and wet state. All samples were deformed to 485% at 192% min^{-1}, and fixed (dried) by holding constant strains for 3 h at room temperature. Following the fixing step, all samples were unloaded at 192% min^{-1} until the force dropped to zero.

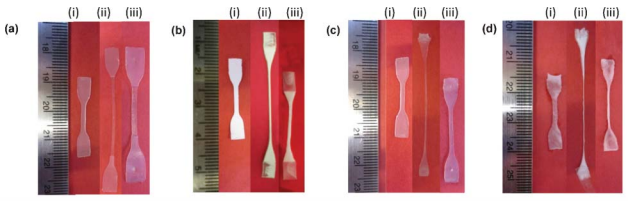

Fig. 7 Water-triggered shape memory tests of (a) dry film, (b) dry web, (c) wet film, and (d) wet web. (i) original dogbone samples; (ii) stretched and fixed samples by Linkam (S/F); and (iii) samples after stretching, fixing and water recovery at room temperature (S/F/R).

room temperature for 10 min to trigger shape recovery. Fig. 7 shows the picture of original dogbone samples, stretched and fixed samples (abbreviated as ''S/F''), and samples after stretching, fixing and water recovery (abbreviated as ''S/F/R''). The corresponding recovery ratios (R_r) are reported in Table 4. Partial recovery was achieved for the dry film with R_r = 44%. The recovery ratio of the dry web significantly increased to 64% compared with the dry film. The larger surface expansion of the bulk film in water accounts for its lower recovery ratio. By programming the samples in the hydrogel state, their recovery ratios greatly improved to 73% (film) and 83% (web). We postulate that for the wet samples, the PCL phase did not deform (or experienced limited deformation) upon tensile deformation and thus resulted in better recovery. This postulation was confirmed by our X-ray study, as revealed below.

The microphase morphologies of PCL–PEG TPUs at original state, deformed state and water-recovered state were characterized using wide angle X-ray scattering (WAXS). 2D WAXS patterns are shown in Fig. 8, and the corresponding diffractogram is shown in Fig. S6, ESI†. The crystal structures of PCL and PEG are well studied in the literature.[25,26] There are three strong reflections in PCL–PEG copolymers, as shown in Fig. 8a-i. Peak 1 is from the (120) reflection of the PEG monoclinic unit cell with *d*-spacing of 4.6 Å (2θ = 19.3°), and Peak 2 is attributed to the (110) plane of the PCL orthorhombic unit cell with *d*-spacing of 4.1 Å (2θ = 21.5°). Peak 3 is located at 2θ = 23.5°, corresponding to *d*-spacing of 3.8 Å. It is the superposition of (200) planes of PCL crystallites and diverse PEG reflections. The diffraction images of the original bulk film and e-spun web (Fig. 8a-i, 8b-i) show uniform intensity distributions for all three rings, suggesting that the PCL and PEG crystallites have no preferred orientation after hot-press

Table 4 Summary of fixing ratios (R_f %) and recovery ratios (R_r %) of e-spun webs and hot-press films. All samples were deformed by Linkam, fixed for 3 h, and recovered in water at RT

Samples	R_f (%)	R_r (%)
Dry films	77 ± 2	44 ± 3
Dry webs	70 ± 3	64 ± 2
Wet films	89 ± 1	73 ± 2
Wet webs	91 ± 1	83 ± 8

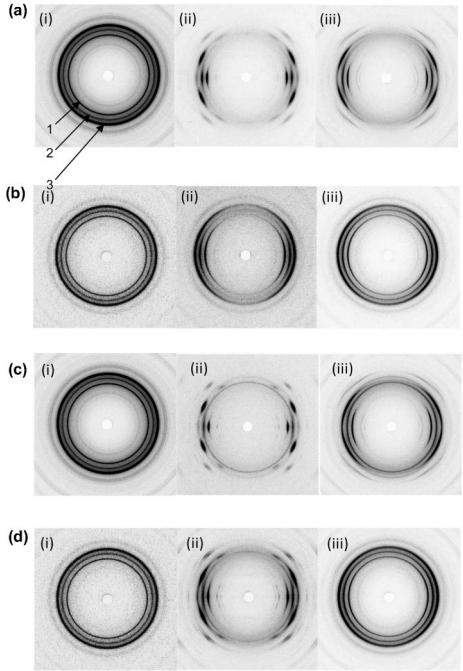

Fig. 8 2D WAXS patterns of (a) dry films, (b) dry webs, (c) wet films, and (d) wet webs. (i) original dogbone samples; (ii) stretched and fixed samples by Linkam (S/F); and (iii) samples which were stretched, fixed, water recovered and dried (S/F/R/D). Strain axis is vertical.

molding or electrospinning. After stretching at RT, Peak 1 and 2 of dry film showed strong equatorial orientation bands, indicating that both PEG and PCL crystallites were deformed and oriented preferentially parallel to the direction of strain (Fig. 8a-ii). Peak 3 showed orientation bands at several azimuthal angles, belonging to diverse PEG plane. After water recovery and complete drying (S/F/R/D), the orientation bands for all three peaks became wider, indicating partial recovery (Fig. 8a-iii). We postulate that the PEG phase completely recovered in water; however upon drying, the PEG block recrystallized in a confined space of orientated PCL phase, which led to the orientation of the PEG phase. Comparing with the dry film (S/F, Fig. 8a-ii), it is observed that Peak 1 decreased in breadth in the wet film (S/F, Fig. 8c-ii), indicating higher orientation of PEG phase, corresponding to larger strains and therefore higher fixing ratio (Table 4). Quite interestingly, the PCL reflection (Peak 2, S/F, Fig. 8c-ii) was almost isotropic, with very weak intensity maximum located on the equator. This observation agrees well with our original ''hydrogel shape memory'' hypothesis (Fig. 5). The orientation of both phases after water recovery (S/F/R/D, Fig. 8c-iii) was attributed to the microstructure reconstruction during recrystallization, as discussed before. The three peaks for the dry web at the stretched state show weak equatorial intensity maximums, suggesting a slightly preferred orientation of both blocks parallel to the stretching direction (Fig. 8b-ii). The lower orientation for the dry web is thought to result from the imperfect fiber orientation after stretching. Comparing the dry web (S/F, Fig. 8b-ii) with wet web in the stretched state (S/F, Fig. 8d-ii), the PEG phase (Peak 1) of wet web was much more oriented than that of the dry web, while the degree of orientation of their PCL phases did not exhibit significant difference. Again, this observation confirmed our hypothesis and is consistent with the higher R_f of the wet web. The higher recovery ratios of wet web and wet film were reflected in a lower degree of orientation of both crystalline phases at the recovered state (S/F/W/D). The intensity for each reflection was plotted *versus* azimuthal angle and the results are given in Fig. S7, ESI†. The crystal orientation was further quantified using Herman's orientation function (f) and full-width at half maximum (FWHM) of the azimuthal spread, shown in Fig. S8, ESI†. It is noted that no peaks shifted position in the intensity *versus* two theta traces, indicating that the d-spacing of all reflections remained the same at different states or by using different deformation methods (dry-stretch or wet-stretch) (Fig. S6, ESI†).

Furthermore, we investigated recovery behaviors of hot-pressed films by varying film thickness to elucidate the water-induced recovery mechanism of PCL–PEG TPUs. A light weight (m = 3 g, corresponding to a stress of 52 kPa) was hung on one end of samples strained as previously described to keep them straight during recovery. Specimens were vertically immersed into water for recovery and the whole recovery process was captured by a high-speed camera. Time ''0'' was taken when the lower end of the sample first touching water. The recovery profiles of pre-stretched films with different thicknesses were shown in Fig. 9a. The recovery time decreased from 300 s to 20 s by decreasing the film thickness from 430 μm to 100 μm. The recovery data were further analyzed by fitting the datasets shown in Fig. 9a with a standard sigmoidal function:

$$R(t) = R_0 + \frac{R_\infty}{1 + e^{-(t-t_0)/\tau}} \quad (5)$$

where R_∞, R_0, t_0 and τ are the four fitting parameters. The fit curves are shown as the solid lines in Fig. 9a with R^2 values from 0.991 to 0.998. Log τ was plotted with log d (here d is the thickness of the films) with a constrained slope of 2. R^2 value was obtained as 0.946 (Fig. 9b). Considering $\tau = k \times d^2/D$, it is apparent that water recovery of our TPUs system is diffusion-dominated.

Finally, the recovery kinetics of micro-fibrous webs were investigated to test the hypothesis that a reduction of the diffusion length to micro scale leads to the substantial increase in the water triggering recovery speed. The recovery behaviors of bulk films are shown for comparison. Four specimens tested here (dry film, dry web, wet film and wet web), were programmed based on the method described in Fig. 6. We observed that the elongated dry film completed recovery in 45 s with a recovery ratio of 42% (Fig. 10a). When changing the material structure from bulk film to micro fibers, remarkably, the recovery time (t_r, time taken for the shape recovery) significantly decreased to 1.3 s by decreasing the diffusion distance substantially (Fig. 10b). By changing the programming method from ''dry drawing'' to ''wet drawing'',

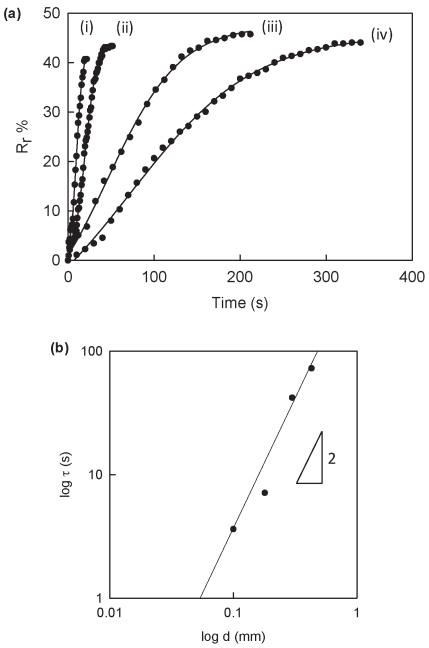

Fig. 9 Water-triggered shape recovery of pre-deformed hot-pressed films (hpf) in water: (a) recovery profiles of hpf with four different thickness of (i) 100 μm, (ii) 180 μm, (iii) 300 μm and (iv) 430 μm. The solid lines are fit curves using a four-parameter sigmoidal function. (b) plot of log τ *vs.* log d for the hpf with four thicknesses. The solid line is fit by linear regression with constrained slope of 2.

the film exhibited a slower recovery speed (t_r = 60 s) (Fig. 10c), which is attributed to higher strain stored in the wet film. Comparing the recovery profiles of the wet web (Fig. 10d) with the dry web, the recovery speed of the wet web was significantly slower (t_r = 25 s). This observation may be the result of two effects. First is the higher fixing ratio of the wet

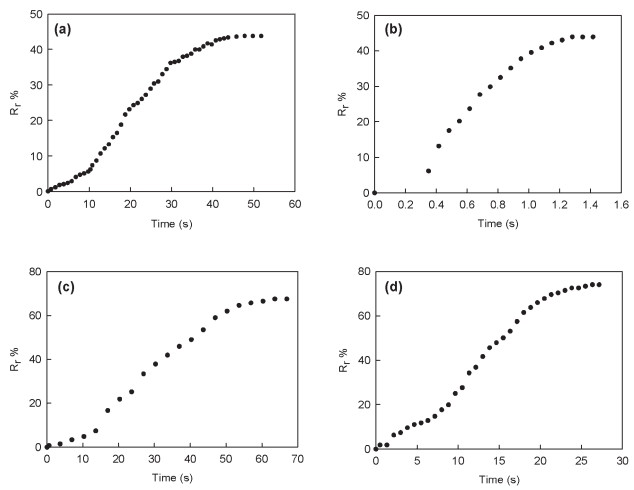

Fig. 10 Water-triggered recovery profiles e-spun webs and hpf: (a) dry film, (b) dry web, (c) wet film and (d) wet web. All four samples were stretched to 485%, and fixed for 3 h at room temperature. For all samples, time ''0'' is when the lower end of the sample first touching water. For (b), the 2nd data point was collected when the whole sample was immersed in water.

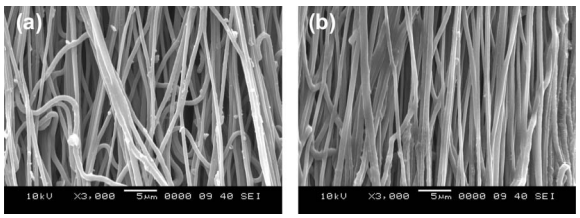

Fig. 11 Scanning electron microscopy (SEM) images of fibrous mats: (a) dry mat after stretching and fixing for 3 h, and (b) wet mat after stretching and fixing (drying) for 3 h. Strain axis is vertical.

web. The higher fixing ratio leads to a more oriented fiber morphology, as shown in Fig. 11. Another more important reason is that upon water absorption, the surface tension of water pulled the fibers together; therefore a more compact fiber morphology formed (*i.e.* lower degree of porosity) (Fig. 11b), potentially slowing water penetration. Instead of presenting a typical ''S'' shape as other shape memory systems,[27,28] the wet web sample showed a ''two-stage'' recovery, where first stage ended at around 20% of total recovery time (Fig. 10d). It is thought that during the first stage, the water molecules permeated into the matrix of the fibrous mats through the pores, resulting in a small amount of recovery (15%); during the second stage, water penetrated into fibers by diffusion, where most of the recovery completed. It is noted that some sample recovery occurred during the immersion process. Due to the strikingly fast recovery, the 2nd data point for the dry web was collected when the upper end of the specimen was fully immersed in water, in order to reflect the recovery behavior of the whole sample (Fig. 10b). In other words, the time gap between the first and second data point for the dry web depends on immersion (dunking) speed. Real-time movies of recovery of all four samples can be found in Supporting Information. As one of our future studies, the water-triggered recovery will be further investigated on e-spun fibrous mats with different fiber diameters. It is expected that smaller fiber diameters yield mats with lower porosity and smaller pore size, which would result in slower recovery.

Conclusions

Water responsive shape memory polymers (SMP), PCL–PEG TPUs, have been demonstrated to feature controllable recovery speed, with the recovery time varying from 1.3 s to 5 min by changing the material form (bulk film *vs.* e-spun webs) and the sample thickness. The water uptake of this series of materials was tailored from 26% to 311% by varying the composition. The fixing and recovery ratios could be greatly improved by deforming the materials in the hydrogel state and later fixed *via* PEG recrystallization during drying. X-ray analysis proved that for the hydrogel samples, the hydrophobic PCL phase underwent limited deformation during stretch which later benefited the recovery. The new ''hydrogel shape memory'' cycle is expected to be applicable to any shape memory

hydrogel system. Owing to its fast and controllable actuation, and high recoverable strain, this class of SMPs offers great potential for applications encompassing water responsive sensors, actuators, and medical devices.

Acknowledgements

The authors thank Prof. Lawrence L. Tavlarides (Syracuse University) for access to the high speed camera in his lab and Dr Ronghong Lin for the help with the experiments. Financial supports from Baxter Healthcare and the New York State Office of Science, Technology and Academic Research (NYSTAR) (CON01587) are gratefully acknowledged.

References

1 C. Liu, H. Qin and P. T. Mather, *J. Mater. Chem.*, 2007, **17**, 1543–1558.
2 A. Lendlein, H. Y. Jiang, O. Junger and R. Langer, *Nature*, 2005, **434**, 879–882.
3 X. F. Luo and P. T. Mather, *Soft Matter*, 2010, **6**, 2146–2149.
4 R. Mohr, K. Kratz, T. Weigel, M. Lucka-Gabor, M. Moneke and A. Lendlein, *Proc. Natl. Acad. Sci. U. S. A.*, 2006, **103**, 3540–3545.
5 W. M. Huang, B. Yang, L. An, C. Li and Y. S. Chan, *Applied Physics Letters*, 2005, **86.**
6 B. Yang, W. H. Huang, C. Li, C. M. Lee and L. Li, *Smart Mater. Struct.*, 2004, **13**, 191–195.
7 B. Yang, W. M. Huang, C. Li and L. Li, *Polymer*, 2006, **47**, 1348–1356.
8 B. Yang, W. M. Huang, C. Li and J. H. Chor, *Eur. Polym. J.*, 2005, **41**, 1123–1128.
9 Y. C. Jung, H. H. So and J. W. Cho, *J. Macromol. Sci., Part B: Phys.*, 2006, **45**, 453–461, and erratum.
10 M. C. Chen, H. W. Tsai, Y. Chang, W. Y. Lai, F. L. Mi, C. T. Liu, H. S. Wong and H. W. Sung, *Biomacromolecules*, 2007, **8**, 2774–2780.
11 H. B. Lv, J. S. Leng, Y. J. Liu and S. Y. Du, *Adv. Eng. Mater.*, 2008, **10**, 592–595.
12 H. B. Lu, Y. J. Liu, J. S. Leng and S. Y. Du, *Smart Materials & Structures*, 2009, **18.**
13 X. Gu and P. T. Mather, *Polymer*, 2012, **53**, 5924–5934.
14 X. F. Luo and P. T. Mather, *Macromolecules*, 2009, **42**, 7251–7253.
15 D. Li and Y. N. Xia, *Adv. Mater.*, 2004, **16**, 1151–1170.
16 D. H. Reneker and A. L. Yarin, *Polymer*, 2008, **49**, 2387–2425.
17 J. Wu, S. Y. Hou, D. C. Ren and P. T. Mather, *Biomacromolecules*, 2009, **10**, 2686–2693.
18 J. W. Lu, Z. P. Zhang, X. Z. Ren, Y. Z. Chen, J. Yu and Z. X. Guo, *Macromolecules*, 2008, **41**, 3762–3764.
19 W. K. Wan, G. Campbell, Z. F. Zhang, A. J. Hui and D. R. Boughner, *J. Biomed. Mater. Res.*, 2002, **63**, 854–861.
20 J. S. Temenoff, K. A. Athanasiou, R. G. LeBaron and A. G. Mikos, *J. Biomed. Mater. Res.*, 2002, **59**, 429–437.
21 J. A. Burdick, C. Chung, X. Q. Jia, M. A. Randolph and R. Langer, *Biomacromolecules*, 2005, **6**, 386–391.
22 V. Normand, D. L. Lootens, E. Amici, K. P. Plucknett and P. Aymard, *Biomacromolecules*, 2000, **1**, 730–738.
23 B. A. Roeder, K. Kokini, J. E. Sturgis, J. P. Robinson and S. L. Voytik-Harbin, *J. Biomech. Eng.*, 2002, **124**, 214–222.
24 J. L. Drury, R. G. Dennis and D. J. Mooney, *Biomaterials*, 2004, **25**, 3187–3199.
25 L. Zhu, S. Z. D. Cheng, B. H. Calhoun, Q. Ge, R. P. Quirk, E. L. Thomas, B. S. Hsiao, F. J. Yeh and B. Lotz, *J. Am. Chem. Soc.*, 2000, **122**, 5957–5967.
26 H. L. Hu and D. L. Dorset, *Macromolecules*, 1990, **23**, 4604–4607.
27 H. Y. Du and J. H. Zhang, *Soft Matter*, 2010, **6**, 3370–3376.
28 I. S. Kolesov, K. Kratz, A. Lendlein and H. J. Radusch, *Polymer*, 2009, **50**, 5490–5498.